6-7 Luglio 2023

Dipartimento di Scienze della Terra, La Sapienza Università di Roma

PRIN 2017

***"Fibres: a multidisciplinary mineralogical, crystal-chemical and biological project to amend the paradigm of toxicity and cancerogenicity of mineral fibres"* (Prot. 20173X8WA4).**

Work-shop "Tossicità e cancerogenicità delle fibre minerali. Un aggiornamento"

Unità

Università di Modena e Reggio Emilia

Introduzione – attività di ricerca unità UNIMORE svolta

Filone di ricerca principale

Correlazione **parametri del modello di tossicità/cancerogenicità** del crisotilo russo, crocidolite e wollastonite → ***adverse effects*** → **10 parametri IARC** KCs (*pathobiological effects*)

Journey to the centre of the lung. The perspective of a mineralogist on the carcinogenic effects of mineral fibres in the lungs Gualtieri, A.F. *Journal of Hazardous Materials,* 2023, 442, 130077.

The Acute Toxicity of Mineral Fibres: A Systematic In Vitro Study Using Different THP-1 Macrophage Phenotypes. Mirata, S., et al., *International Journal of Molecular Sciences*, 2022, 23(5), 2840.

Acute cytotoxicity of mineral fibres observed by time-lapse video microscopy. Di Giuseppe, D., et al., *Toxicology*, 2022, 466, 153081.

Characterization of fibrous wollastonite NYAD G in view of its use as negative standard for in vitro toxicity tests. Di Giuseppe D., et al., *Minerals*, 2021, 11(12), 1378.

WebFPTI: A tool to predict the toxicity/pathogenicity of mineral fibres including asbestos. Gualtieri, A.F., et al., *Earth Science Informatics*, 2021, 14(4), pp. 2401–2409.

Characterization and assessment of the potential toxicity/pathogenicity of Russian commercial chrysotile. Di Giuseppe, D. et al., . *American Mineralogist*, 2021, 106(10), pp. 1606–1621.

Bridging the gap between toxicity and carcinogenicity of mineral fibres by connecting the fibre crystal-chemical and physical parameters to the key characteristics of cancer. Gualtieri, A.F. *Current Research in Toxicology*, 2021, 2, pp. 42–52.

Lung cancer: Mechanisms of carcinogenesis by asbestos. Mossman, B.T., Gualtieri, A.F. *Occupational Cancers*, 2020, pp. 239–26.

Introduzione – attività di ricerca unità UNIMORE svolta

Caratterizzazione e tossicità di fibre minerali in collaborazione con le altre unità di ricerca

The crystal structure of the killer fibre erionite from Tuzköy (Cappadocia, Turkey). Giacobbe, C. et al., IUCrJ, 10(4).

Identification of iron compounds in chrysotile from the Balangero mine (Turin, Italy) by micro-Raman spectroscopy Fornasini, L., et al., Journal of Raman Spectroscopy, 2022, 53(11), pp. 1931–1941.

Characterisation of potentially toxic natural fibrous zeolites by means of electron paramagnetic resonance spectroscopy and morphological-mineralogical studies. Giordani M., et al., Chemosphere, 2022, 291, 133067.

In vitro toxicity of fibrous glaucophane. Gualtieri A.F. et al., Toxicology, 2021, 454, 152743.

Crystal structure determination of a lifelong biopersistent asbestos fibre using single-crystal synchrotron X-ray micro-diffraction. Giacobbe C. et al., IUCrJ, 2021, 8, pp. 76–86.

Characterization and assessment of the potential toxicity/pathogenicity of fibrous glaucophane. Di Giuseppe D., et al., Environmental Research, 2019, 178, 108723.

- Rilascio metalli da fibre minerali con UNIPI-PR e UNIGE con esperimenti a ESRF ed ELETTRA
- *Cross talk* del Ca++ dall'erionite con UNIPI-PR e UNIGE con esperimenti a ESRF ed ELETTRA ed esperimenti di concentrazione Ca/Na nel cytosol

Filone di ricerca principale

Parametri cristallochimici-fisici del crisotilo russo, crocidolite e wollastonite

⇓

Effetti avversi in vitro *(adverse effects)*

⇓

10 parametri IARC KCs (*pathobiological effects*)

Filone di ricerca principale

Correlare i **parametri cristallochimici/fisici delle fibre minerali** crisotilo russo (fibra corta e lunga), crocidolite e wollastonite → "**effetti avversi *in vitro***" → **10 parametri IARC che descrivono la cancerogenesi**

'10 key characteristics (KCs) of carcinogens', the properties of a cancer-causing agent (Guyton et al., 2018) to evaluate the carcinogenic potency*:*

Characteristic	Examples of relevant evidence
1. Is electrophilic or can be metabolically activated	Parent compound or metabolite with an electrophilic structure (e.g. epoxide, quinone, etc.), formation of DNA and protein adducts
2. Is genotoxic	DNA damage (DNA strand breaks, DNA–protein cross-links, unscheduled DNA synthesis), intercalation, gene mutations, cytogenetic changes (e.g. chromosome aberrations, micronuclei)
3. Alters DNA repair or causes genomic instability	Alterations of DNA replication or repair (e.g. topoisomerase II, base-excision or double-strand break repair)
4. Induces epigenetic alterations	DNA methylation, histone modification, microRNA expression
5. Induces oxidative stress	Oxygen radicals, oxidative stress, oxidative damage to macromolecules (e.g. DNA, lipids)
6. Induces chronic inflammation	Elevated white blood cells, myeloperoxidase activity, altered cytokine and/or chemokine production
7. Is immunosuppressive	Decreased immunosurveillance, immune system dysfunction
8. Modulates receptor-mediated effects	Receptor in/activation (e.g. ER, PPAR, AhR) or modulation of exogenous ligands (including hormones)
9. Causes immortalization	Inhibition of senescence, cell transformation
10. Alters cell proliferation, cell death or nutrient supply	Increased proliferation, decreased apoptosis, changes in growth factors, energetics and signaling pathways related to cellular replication or cell cycle control, angiogenesis

Filone di ricerca principale

Alessandro F. Gualtieri Current Research in Toxicology 2 (2021) 42–52

Parameter	Element	Major adverse effect
Morphometric		
length L	(1,1)	frustrated phagocytosis
diameter D	(1,2)	frustrated phagocytosis
crystal curvature	(1,3)	reduced surface adhesion of proteins/cells
crystal habit	(1,4)	airways deposition depth
fiber density	(1,5)	airways deposition depth
hydrophobic character of the surface	(1,6)	Interaction with biopolymers, phagocytosis
surface area	(1,7)	airways deposition depth, frustrated phagocytosis
Chemical		
Total iron content	(1,8)	Production of ROS
ferrous iron	(1,9)	Production of ROS
Surface ferrous iron/iron nuclearity	(1,10)	Production of ROS
content of metals other than iron	(1,11)	Production of ROS
Biodurability		
dissolution rate log(R)	(1,12)	frustrated phagocytosis ...
velocity of iron release	(1,13)	production of ROS
velocity of silica dissolution	(1,14)	production of ROS?
velocity of release of metals	(1,15)	ROS production
Surface activity		
ξ potential	(1,16)	production of ROS and hemolysis
fibers' aggregation	(1,17)	frustrated phagocytosis
Cation exchange in zeolites	(1,18)	interference with ER cross-talk?

IARC's 10 key characteristics of carcinogens
Characteristic
1. Is electrophilic or can be metabolically activated
2. Is genotoxic
3. Alters DNA repair or causes genomic instability
4. Induces epigenetic alterations
5. Induces oxidative stress
6. Induces chronic inflammation
7. Is immunosuppressive
8. Modulates receptor-mediated effects
9. Causes immortalization
10. Alters cell proliferation, cell death or nutrient supply

Filone di ricerca principale

Alessandro F. Gualtieri Current Research in Toxicology 2 (2021) 42–52

Table 3
Key characteristics/pathological process known to cause cancer in humans. For each patho-biological process featuring the 10 IARC key characteristics (Smith et al., 2016), the major adverse effects induced by specific fibre' parameters (see the list in Table 1) are reported.

Fibre parameter	Major adverse effect	Key characteristic of carcinogenicity (patho-biological process)
length (1,1)	Prompts indirect production of electrophilic species like hydroxyl radicals (ROS) due to alveolar macrophages (AM) frustrated phagocytosis	1. electrophilicity
surface area (1,7)	Rules the overall size of the fibre *in vivo* with indirect production of ROS if the fibre is long enough to cause frustrated phagocytosis	
total iron content (1,8)	Prompt direct production of electrophilic species like hydroxyl radicals ROS by metal-mediated Fenton type reaction at the fibre' surface	
ferrous iron (1,9)		
surface ferrous iron (1,10)		
content of metals other than iron (1,11)		
dissolution rate (1,12)	Rules the length of the fibre *in vivo* with indirect production of ROS if the fibre is long enough to cause frustrated phagocytosis	
velocity of iron release (1,13)	Rule the rate of (direct) production of ROS at the fibre' surface or at the surface of newly-formed silica relicts (e.g. after dissolution of chrysotile: Gualtieri et al., 2019c)	
velocity of silica release/formation (1,14)		
velocity of release of metals (1,15)		
length (1,1)	Prompts indirect production of genotoxic ROS/RNS (reactive nitrogen species) during AM frustrated phagocytosis	2. genotoxicity
surface area (1,7)	Rules the overall size of the fibre *in vivo* with indirect production of genotoxic ROS/RNS if the fibre is long enough to cause frustrated phagocytosis	
total iron content (1,8)	Prompt direct production of genotoxic ROS by metal-mediated Fenton type reaction at the fibre' surface	
ferrous iron (1,9)		
surface ferrous iron (1,10)		
content of metals other than iron (1,11)		
dissolution rate (1,12)	Rules the length of the fibre *in vivo* with indirect production of genotoxic ROS/RNS if the fibre is long enough to cause frustrated phagocytosis	
velocity of iron release (1,13)	Rule the rate of (direct) production of genotoxic ROS/RNS at the fibre' surface or at the surface of newly-formed silica metastable products	
velocity of silica release/formation (1,14)		
velocity of release of metals (1,15)		
zeta potential (1,16)	Rules the production of genotoxic ROS/RNS at the fibre' surface	

⋮

Major patho-biological process ≡ key characteristic of cancer

Filone di ricerca principale

- raccolta dati *in vitro* relativi a markers IARC 10 KCs su crisotilo russo L≤5μm e L>5μm, crocidolite UICC (standard positivo): e wollastonite NYAD-G (standard negativo) da parte di **UNIGE e UNIVPM** ***In progress***
- classificazione finale delle fibre studiate: quanti **KCs** (da 1 a 10) sono attivi per ogni campione e da quali parametri FPTI vengono generati?

COMET test	wol	cri corto	cri lungo	cro	wol	cri corto	cri lungo	cro	wol	cri corto	cri lungo	cro
tail moment met5a 6h	13	40	100	227	0,13	0,4	1	2,27	0,13	0,4	1	2,27
tail moment met5a 24h	80	70	250	500	0,8	0,7	2,5	5	0,8	0,7	2,5	4,2
tail moment met5a 48h	100	171	168	420	1	1,71	1,68	4,2	1	1,71	1,68	3,3
tail moment A549 6h	75	217	316	330	0,75	2,17	3,16	3,3	0,75	1,25	2	2,31
tail moment A549 24h	62	125	200	231	0,62	1,25	2	2,31	0,62	0,53	0,67	1,53
tail moment A549 48h	60	53	67	153	0,6	0,53	0,67	1,53	0,6			
media					**0,65**	**1,12667**	**1,835**	**3,10167**	0,65	0,918	1,57	2,722
2 genotoxicity									**0,2388**	**0,33725**	**0,57678**	**1**
lenght (1,1)											**0,57678**	**1**
surface area (1,7)										**0,33725**	**0,57678**	
total iron content (1,8)												**1**
ferrous iron (1,9)												**1**
surface ferrous iron (1,10)												**1**
content of metals (1,11)										**0,33725**	**0,57678**	**1**
dissolution rate (1,12)										**0,33725**	**0,57678**	
velocity of iron release (1,13)										**0,33725**	**0,57678**	
velocity of silica formation (1,14)										**0,33725**	**0,57678**	
velocity of release of metals (1,15)										**0,33725**	**0,57678**	
zeta potential (1,16)												**1**

Filone di ricerca principale – modellazione in corso

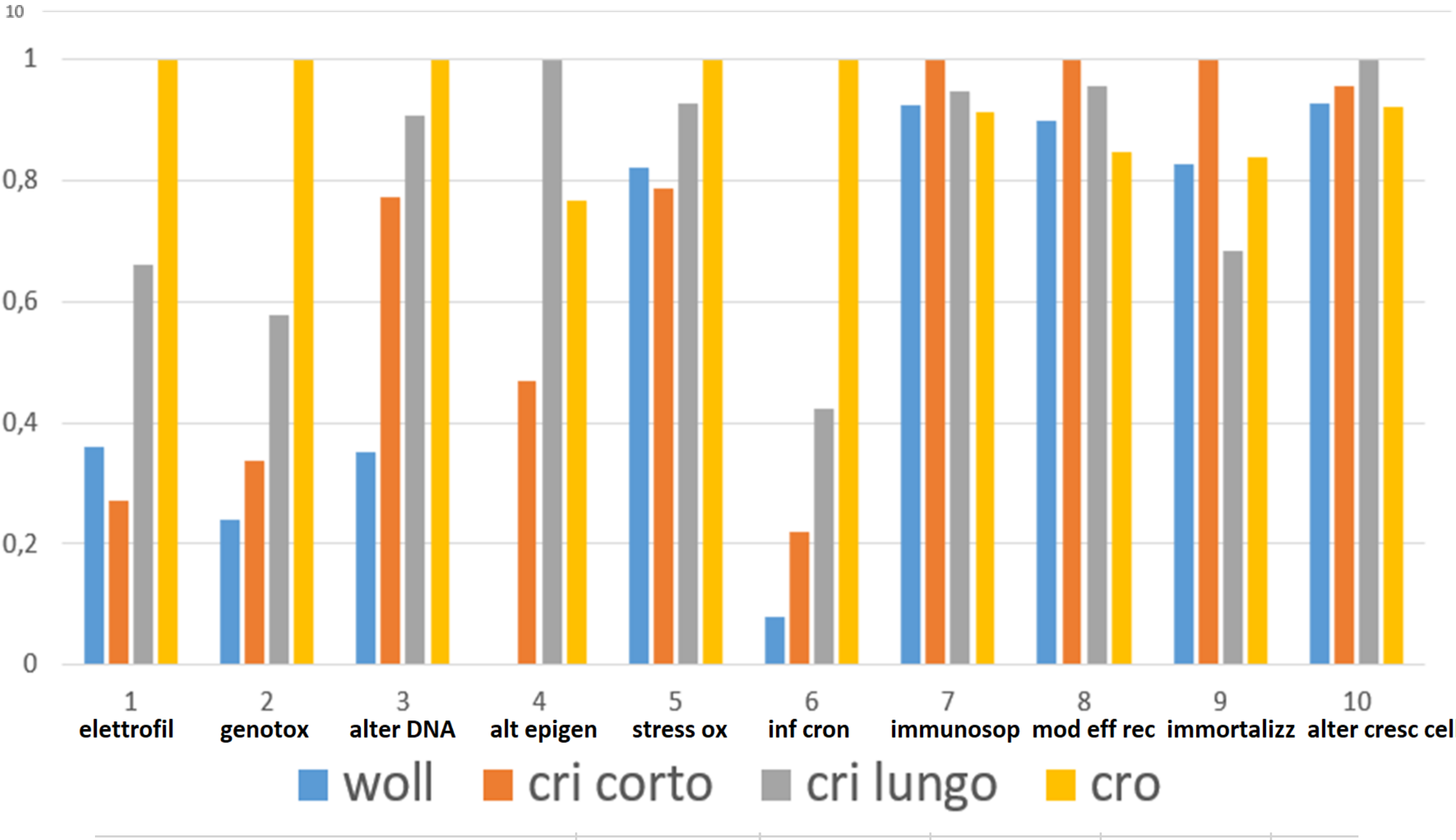

Filone di ricerca principale – modellazione in corso

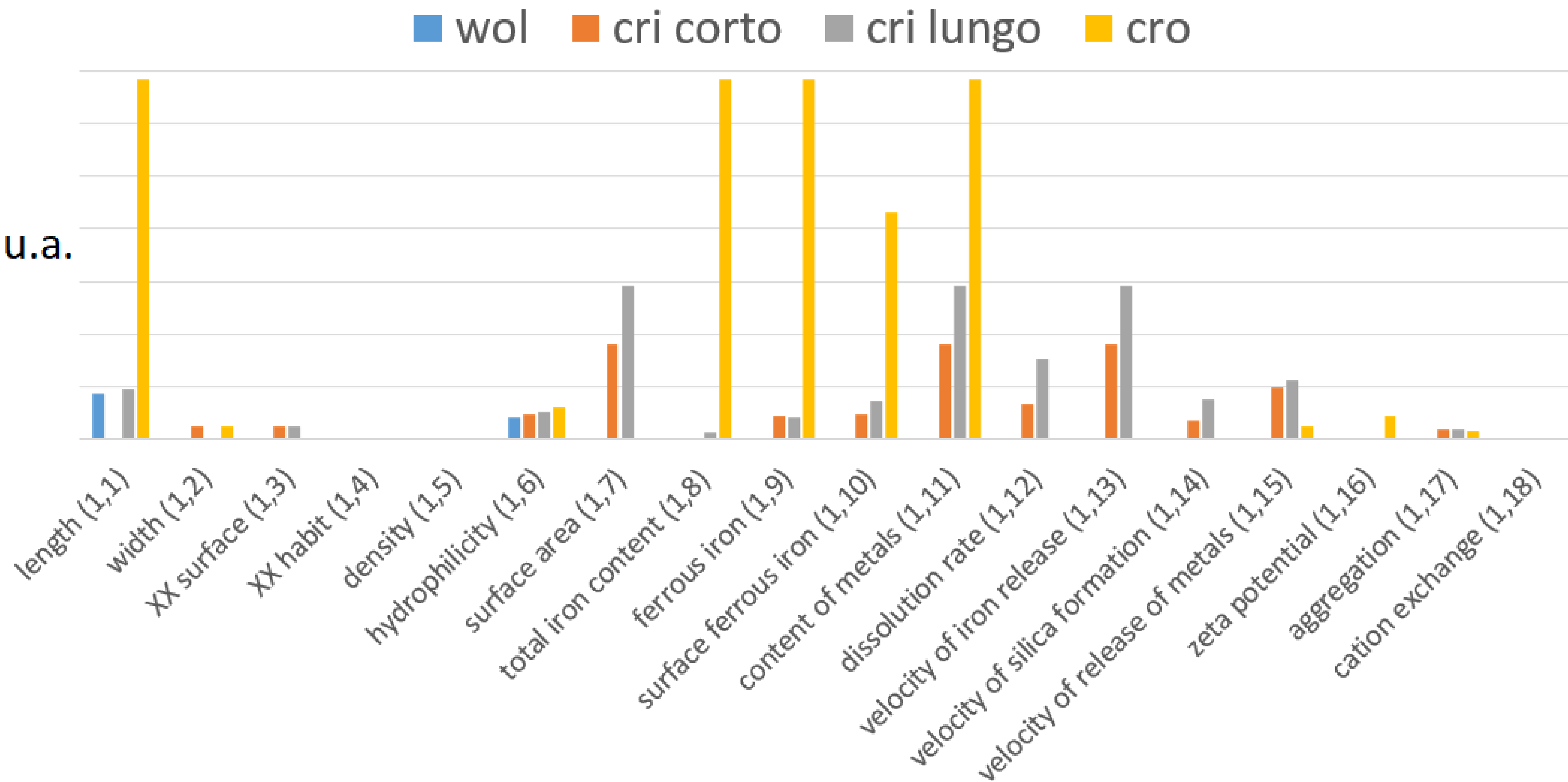

	wol	cri corto	cri lungo	cro
aggregation (1,17)		1,21838	1,37248	1
cation exchange (1,18)				
tot	**7,193521**	**42,9132**	**53,2872**	**52,53**

Filone di ricerca principale

Nuclearità del ferro ed implicazioni per il modello di tossicità delle fibre minerali

Nuclearity of iron in mineral fibres. Determination and implications for toxicity models

- Cyto/genotoxic oxidant species catalysed by iron cause chronic inflammation of mineral fibres. The preferred catalytic active site is when iron forms isolated $(FeO)^{2+}$ structures (nuclearity=1) whereas the catalytic activity is reduced or null when iron forms clusters of higher nuclearity.

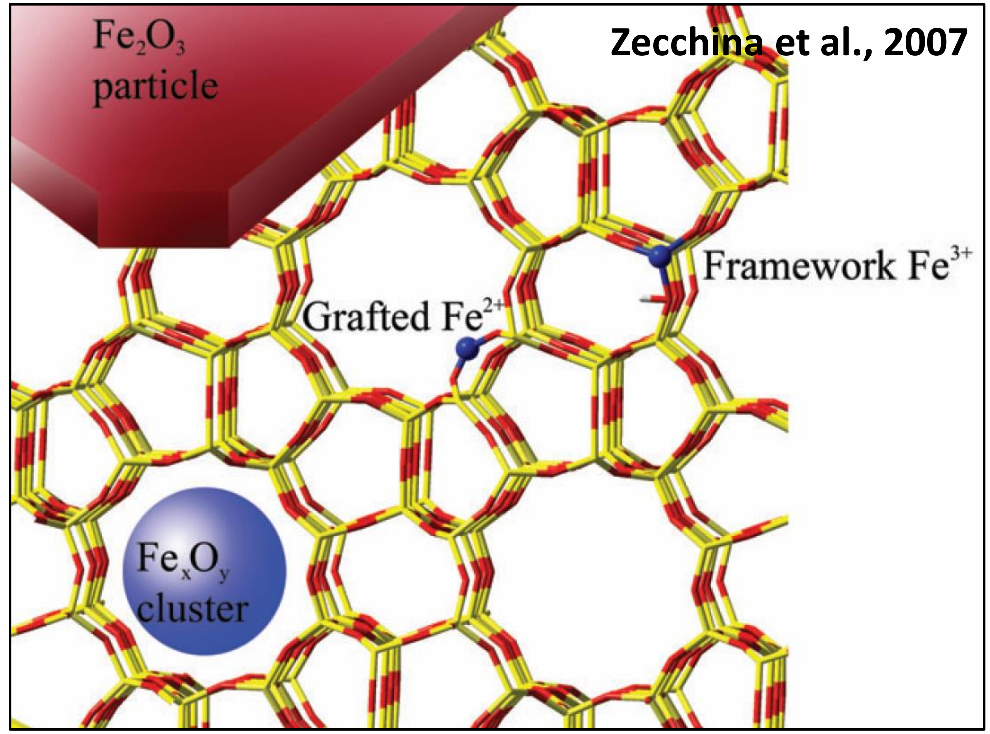

- Iron nuclearity of mineral fibres has been investigated on a suite of standards and fibres to assess the contribution to the models of prediction of the toxicity/carcinogenicity. Approach:

  -*ab initio* **density functional theory (DFT)** calculations (***to be completed***)

  -**multivariate curve resolution (MCR)** applied to the analysis of UV-Vis spectra

Nuclearity of iron in mineral fibres.

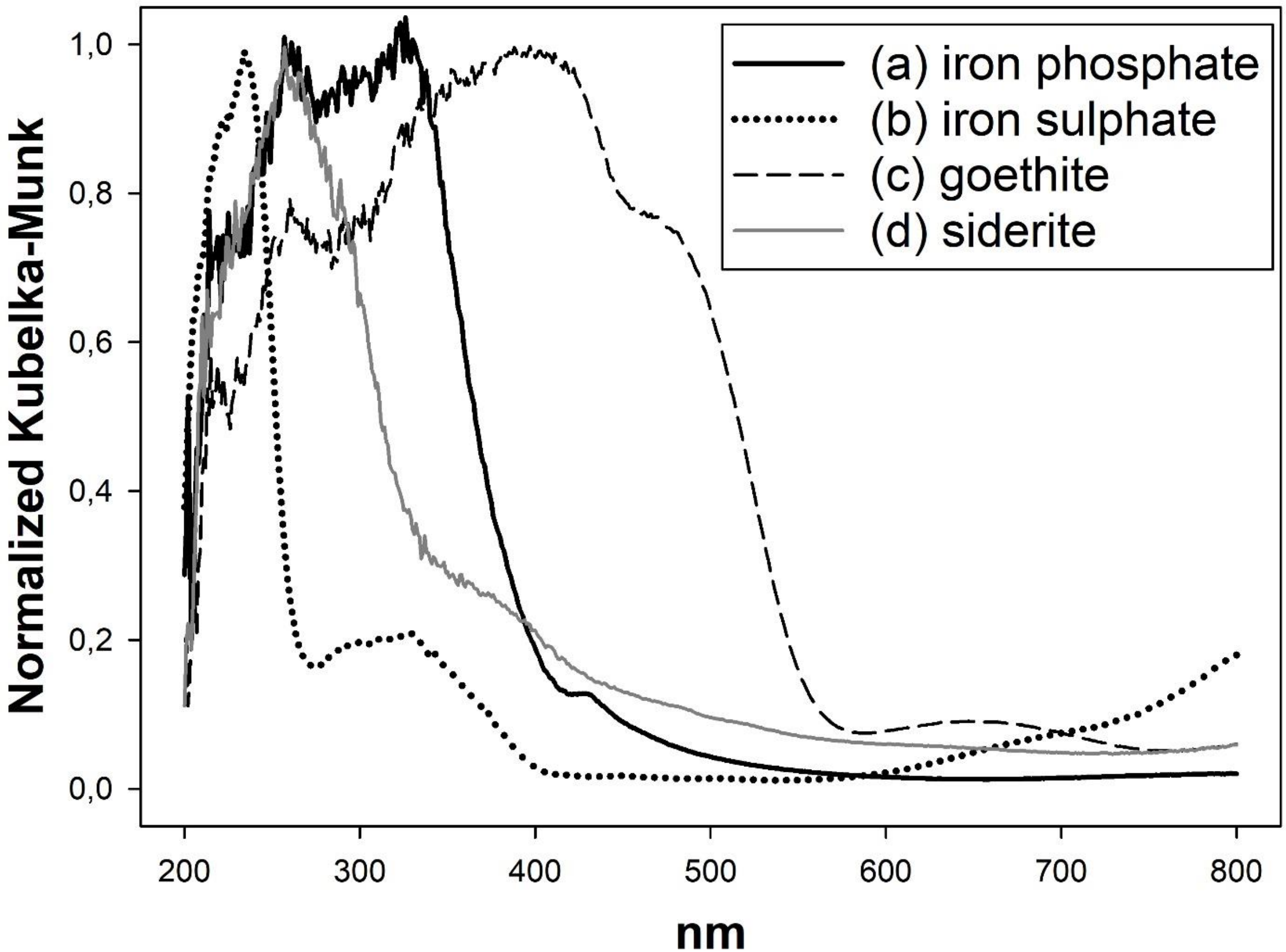

UV-Vis spectra of selected standards with distinctive iron chemical environment. Legend: (a) iron phosphate dihydrate with isolated Fe^{3+} atoms; (b) iron sulphate with isolated Fe^{2+} atoms; (c) goethite ($Fe^{3+}O(OH)$) with a cluster of 6 iron atoms in the second shell; (d) siderite ($Fe^{2+}CO_3$) with a cluster of 6 iron atoms in the second shell and carbon-bonded oxygen atoms in the first shell.

Nuclearity of iron in mineral fibres

sample	origin	sample purity	Fe oxidation state	Fe chemical environment	Fe mass (%)
ammonium iron oxalate trihydrate	Synthetic, Merck	yes	Fe^{3+}	isolated	13.0
ammonium iron sulphate dodecahydrate	Synthetic, Merck	yes	Fe^{2+}	isolated	11.6
goethite	Synthetic, Bayer	yes	Fe^{3+}	Cluster (6 iron atoms in the second shell)	62.9
hematite	Natural, Elba island (Italy)	yes	Fe^{3+}	Cluster (6 iron atoms in the second shell)	69.9
iron chloride	Synthetic, Merck	yes	Fe^{3+}	Cluster (4 iron atoms in the second shell)	34.4
iron phosphate dihydrate	Synthetic, Merck	yes	Fe^{3+}	isolated	27.9
iron sulphate hydrate	Synthetic, Merck	yes	Fe^{3+}	isolated	37.0
iron sulphate heptahydrate	Synthetic, Merck	yes	Fe^{2+}	isolated	36.8
magnetite	Natural, Cogne, Aosta Valley	yes	Fe^{2+}, Fe^{3+}	Cluster (6 iron atoms in the second shell)	72.4
iron	Natural, GEMMA 1786 Modena	yes	Fe	Cluster (6 iron atoms in the second shell)	100.0
kaolinite	Natural, Washington USA	yes	Fe^{3+}	isolated	0.05
olivine	Natural, Balmuccia, Vercelli	yes	Fe^{2+}	dimeric or trimeric	12.3
olivine calcined 1200 °C in air	Natural, Balmuccia, Vercelli	Yes, hematite formed	Fe^{3+}	Cluster (6 iron atoms in the second shell)	12.3
pyrope (iron-containing garnet)	Natural, Piedmont, Italy	yes	Fe^{2+}	Isolated (possibly dimeric?)	6.7
pyroxene (iron-containing diopside)	Natural, GEMMA 1786 Modena	yes	Fe^{2+}	Isolated (possibly dimeric?)	1.0?
siderite	Natural, Fabriano, Marche	yes	Fe^{2+}	Cluster (6 iron atoms in the second shell)	48.2
talc	Borgotaro (Parma, Italy)	yes	Fe^{3+}	Cluster	<0.1

Nuclearity of iron in mineral fibres

Mineral fibres collected in order to predict the iron chemical environment and nuclearity:

- actinolite asbestos from Aurina Valley, Bolzano (Italy)
- amosite from Penge mine, Northern Province (South Africa)
- the UICC standard anthophyllite asbestos (Finnish NB #4173-111-5) from Paakkila (Finland)
- chrysotile from Balangero mine (Turin, Italy)
- commercial chrysotile from Yasniy mine, Orenburg Minerals (Russia)
- the UICC standard crocidolite South African NB #4173-111-3
- fibrous glaucophane from San Anselmo, Marin County (CA, USA);
- tremolite asbestos from the Ultrabasic Lanzo Massif in the Occidental Alps (Lanzo Valley, Piedmont)
- commercial fibrous wollastonite NYAD G from Willsboro-Lewis (New York, USA)

Nuclearity of iron in mineral fibres (*to be completed*)

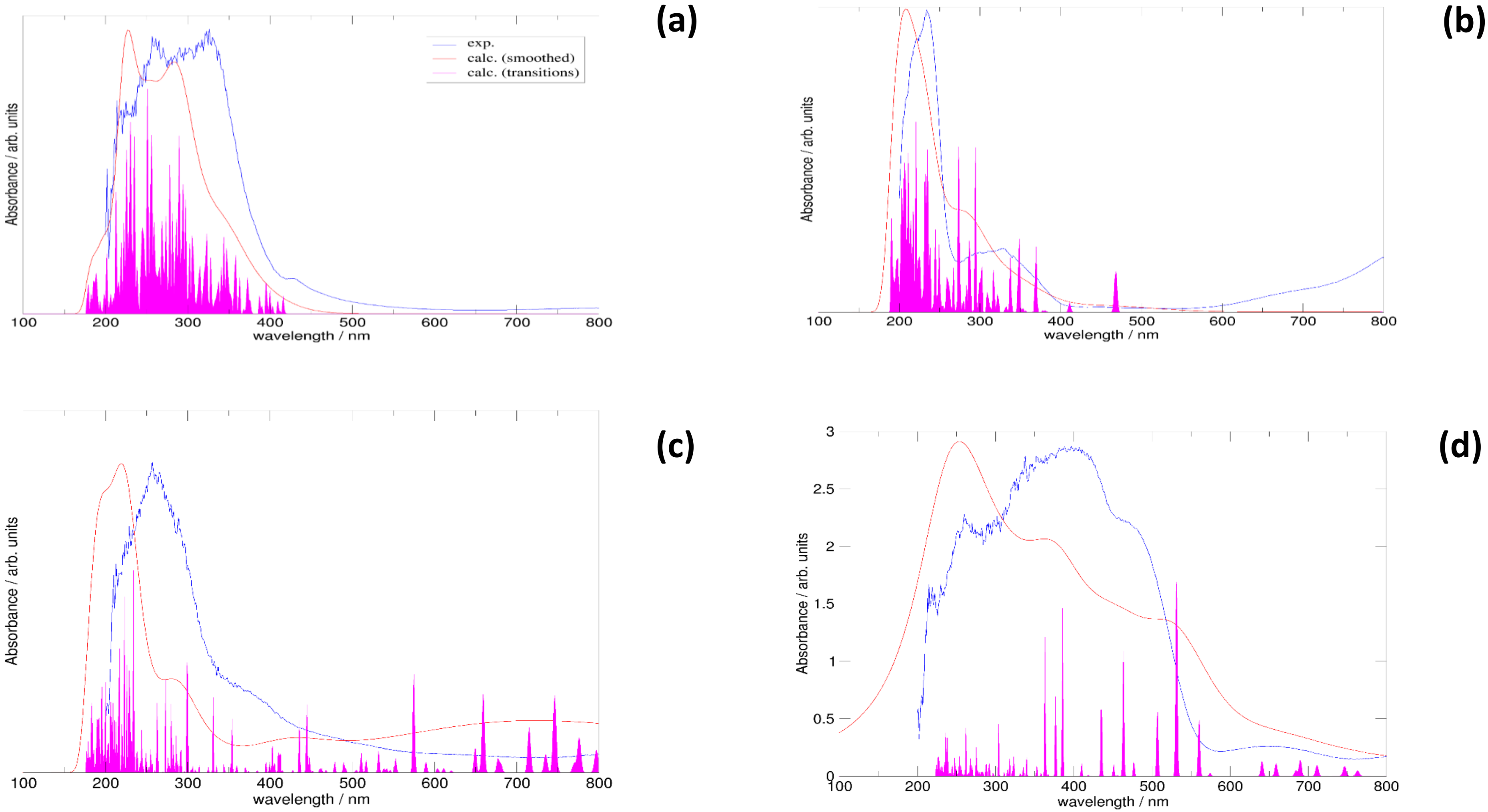

Experimental UV-Vis spectra of: **(a)** Fe^{3+}-phosphate; **(b)** Fe^{2+}-sulphate; **(c)** siderite ($Fe^{2+}CO_3$); **(d)** goethite ($Fe^{3+}O(OH)$) (blue lines) with TD-DFT spectra (red lines) and TD-DFT transitions (magenta spikes).

Nuclearity vs. production og HO$^{\bullet}$ (*DFT modelling to be completed*)

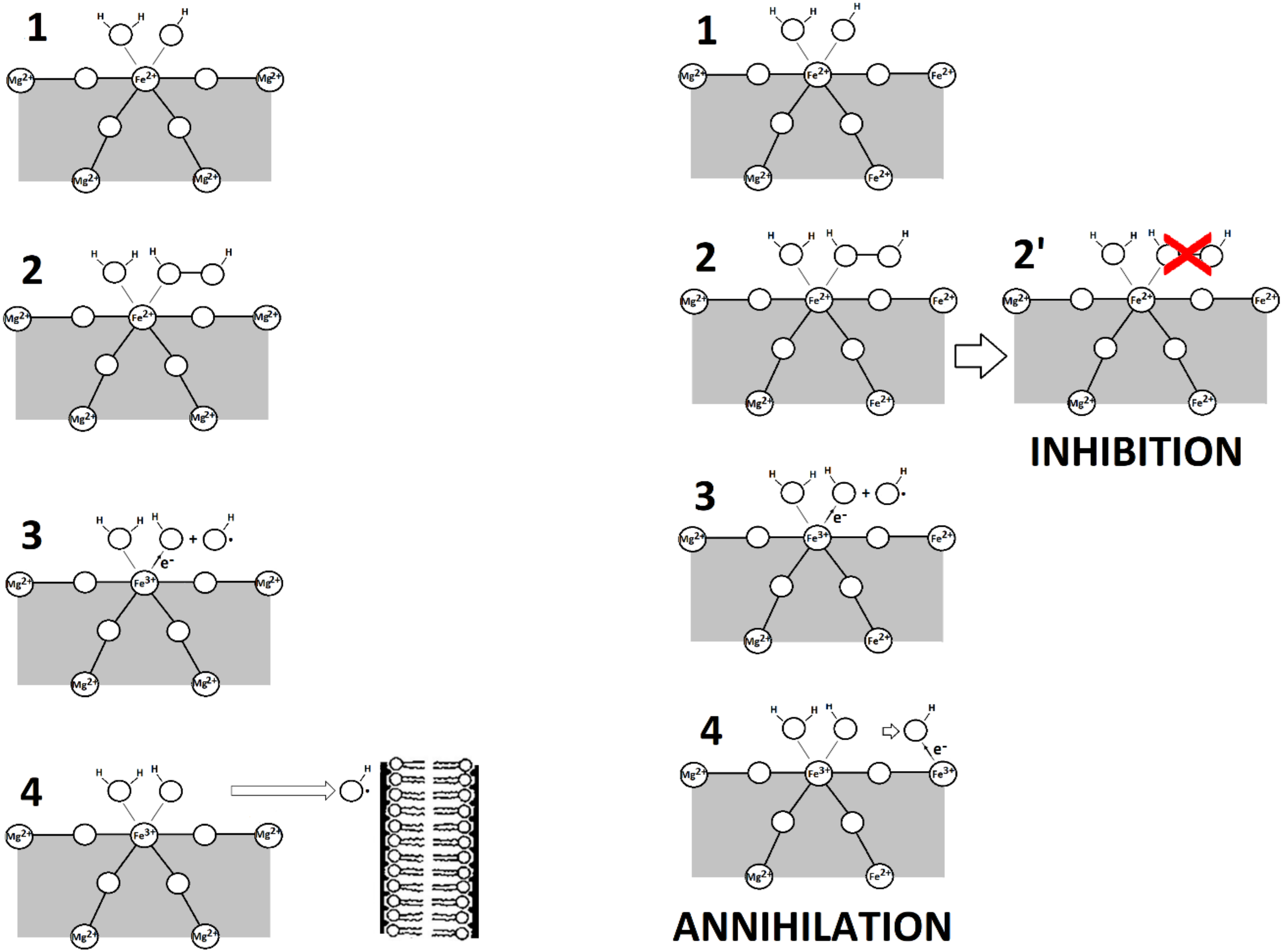

Nuclearity of iron in mineral fibres

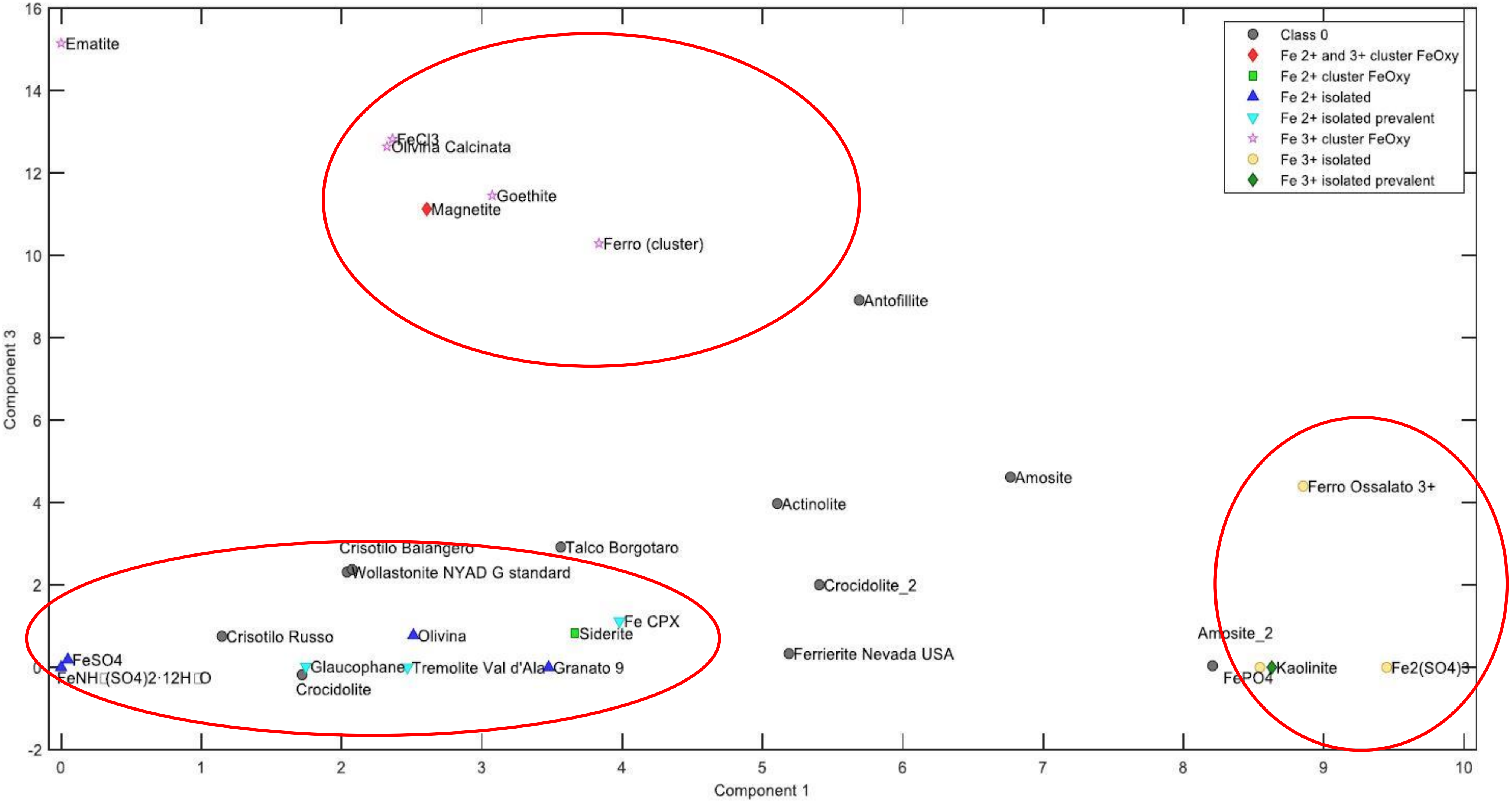

Multivariate Curve Resolution – Alternating Least Squares (MCR-ALS)

(De Juan, 2021; Jaumot, 2015)

Nuclearity of iron in mineral fibres: MCR 2 FPTI

- Preparation of the sample powder (as pure as possible);
- Collect the UV-Vis spectrum, 200-800 nm range, same experimental conditions);
- Data reduction and normalization of the Kubelka-Munk signal;
- MCR analysis for the extraction of the PC parameters for the cluster plots;
- Classification of the sample in terms of the calculated components C1 (isolated Fe^{3+}), C2 (cluster Fe^{2+} and Fe^{3+}), C3 (cluster Fe^{3+}), C4 (isolated Fe^{2+}). Intermediate cases C1-C3 and C4-C2 are possible and interpreted as iron with low nuclearity;
- Assignment of the value of the FPTI nuclearity-related toxicity parameter 1.10:

  C4 (isolated Fe^{2+}) or C1 (isolated Fe^{3+}) $\rightarrow$ Fe^{2+} nuclearity = 1 $\rightarrow$ index value = 0.07 (high toxicity, due to the higher probability of producing hydroxyl radicals);

  C1-C3 or C4-C2 $\rightarrow$ Fe^{2+} nuclearity = 2 $\rightarrow$ index value = 0.03 (low-moderate toxicity);

  C2 (cluster Fe^{2+} and Fe^{3+}) or C3 (cluster Fe^{3+}) $\rightarrow$ Fe^{2+} nuclearity > 2 $\rightarrow$ index value = 0.02 (low toxicity).

American Mineralogist, Volume 83, pages 577–589, 1998

Crystal chemistry of the zeolites erionite and offretite

E. PASSAGLIA,[1] G. ARTIOLI,[2,*] AND A. GUALTIERI[1]

[1]Dipartimento di Scienze della Terra, Università di Modena, via S. Eufemia 19, I-41100 Modena, Italy
[2]Dipartimento di Scienze della Terra, Università di Milano, via Botticelli 23, I-20133 Milano, Italy

ABSTRACT

Many known occurrences of the zeolites erionite and offretite have been characterized by electron probe microanalysis, X-ray powder diffraction, and optical microscopy. For the first time, a substantial amount of experimentally consistent and homogeneous chemical and crystallographic data have been evaluated for these natural zeolites. Systematic analysis of the data, performed by statistical multivariate analysis, leads to the following conclusions: (1) the two zeolites have well-defined compositional fields in the chemical space describing the extraframework cation content, best illustrated in a Mg-Ca(+Na)-K(+Sr+Ba) diagram; (2) no discrimination is possible on the basis of the framework Si/Al ratio because of the extensive compositional overlap between the two species, however the Si-Al content in the framework tetrahedra is the major control on the unit-cell volume dimensions, particularly in erionite; (3) the crystal chemistry of the Mg cations is a major factor in controlling the crystallization of the mineral species; (4) cation compositions at the boundary of the recognized compositional fields might be due to chemical averaging of two-phase intergrowths, although these mixed-phase occurrences are much less common than previously thought; (5) the sign of optical elongation is not a distinctive character of the two phases, it is related to the Si/Al ratio in the framework tetrahedra of each zeolite type and cannot be used for identification purposes; (6) the zeolite mineral species epitaxially overgrown on levyne in all cases is identified as erionite; in a few cases offretite was found to be overgrown on chabazite; (7) erionite samples epitaxially overgrown on levyne are substantially more Al-rich and Mg-poor than the erionite samples associated with other zeolites.